HYPERSPECTRAL UNMIXING ACCOUNTING FOR SPATIAL CORRELATIONS AND ENDMEMBER VARIABILITY

Abderrahim Halimi[(1)]*, Nicolas Dobigeon*[(2)]*, Jean-Yves Tourneret*[(2)] *and Paul Honeine*[(1)]

[(1)] Institut Charles Delaunay (CNRS), Université de technologie de Troyes, Troyes, France.
[(2)] University of Toulouse, IRIT/INP-ENSEEIHT/TéSA, Toulouse, France

ABSTRACT

This paper presents an unsupervised Bayesian algorithm for hyperspectral image unmixing accounting for endmember variability. This variability is obtained by assuming that each pixel is a linear combination of random endmembers weighted by their corresponding abundances. An additive noise is also considered in the proposed model generalizing the normal compositional model. The proposed model is unsupervised since it estimates the abundances and both the mean and the covariance matrix of each endmember. A classification map indicating the class of each pixel is also obtained based on the estimated abundances. Simulations conducted on a real dataset show the potential of the proposed model in terms of unmixing performance for the analysis of hyperspectral images.

Index Terms— Hyperspectral imagery, endmember variability, image classification, Markov chain Monte-Carlo.

1. INTRODUCTION

Unmixing hyperspectral (HS) images consists of decomposing a pixel spectrum into a combination of pure constituent spectra, or endmembers, and a set of corresponding fractions, or abundances. The mixture model associated with spectral unmixing can be linear or nonlinear, depending on the hyperspectral image under consideration [1]. Endmember variability (EV) has been identified as one of the most profound sources of error in abundance estimation [2, 3]. Many algorithms have been proposed to mitigate EV effects. These algorithms are often classified into bundle approaches (that consider each physical material as a set or bundle of spectra) or statistical approaches [2, 3]. The latter assumes random endmembers leading to statistical models such as the beta compositional model [4] and the normal compositional model (NCM) [5–7]. This paper considers a statistical approach based on the generalized NCM (GNCM) initially introduced in [8, 9]. This model introduces an additional noise to the NCM accounting for mismodeling effects. The GNCM considers also a different mean vector and covariance matrix for each endmember to analyze each component separately. Moreover, the GNCM accounts for the spatial correlation between adjacent pixels using Markov random fields (MRFs) as in [10, 11].

In order to estimate the parameters of the GNCM, we investigate a Bayesian approach assuming appropriate prior distributions for the unknown parameters and hyperparameters in order to satisfy the known physical constraints. Since the posterior distribution of this model is quite complicated, we consider a Markov chain Monte-Carlo (MCMC) method which generates samples according to the posterior and computes the standard Bayesian estimators (minimum mean square error (MMSE) and maximum a posteriori (MAP) estimators) using the generated samples. More precisely, we consider a Gibbs sampler coupled with a constrained Hamiltonian Monte Carlo (CHMC) method that has been introduced in [12, Chap. 5] and applied to the non-linear unmixing of HS images in [13].

The paper is structured as follows. The Bayesian model used to unmix HS images in presence of EV is introduced in Section 2. The MCMC approach used to estimate the parameters of this model was detailed in [8, 9] and is thus not presented here. Section 3 analyzes the performance of this approach when applied to a real image. Conclusions and future work are reported in Section 4.

2. A BAYESIAN MODEL EXPLOITING EV

This section first recalls the generalized normal compositional model (GNCM) introduced in [8,9] to account for EV. Second, it introduces the associated Bayesian unmixing strategy that captures the EV and estimates the abundances while considering spatial correlation between adjacent pixels.

2.1. Mixing model

The endmembers generally vary from one pixel to another of the observed image [3]. In this paper, we describe the GNCM that takes into account this variability. This model assumes that the nth pixel spectrum $\boldsymbol{y}_n$ (of size $L\times 1$) is a linear combination of R varying endmembers $\boldsymbol{s}_{rn}$ corrupted by an additive independent and identically distributed (i.i.d.) noise $\boldsymbol{e}_n$ as follows

$$\boldsymbol{y}_n = \sum_{r=1}^{R} a_{rn}\boldsymbol{s}_{rn} + \boldsymbol{e}_n = \boldsymbol{S}_n\boldsymbol{a}_n + \boldsymbol{e}_n \tag{1}$$

where $\boldsymbol{a}_n = [a_{1n}, \cdots, a_{Rn}]^T$ is the $(R \times 1)$ abundance vector of the nth pixel, $\boldsymbol{s}_{rn} \sim \mathcal{N}\left(\boldsymbol{m}_r, \text{diag}\left(\boldsymbol{\sigma}_r^2\right)\right)$ is the rth endmember associated with the nth pixel, $\boldsymbol{S}_n = [\boldsymbol{s}_{1n}, \cdots, \boldsymbol{s}_{Rn}]$, $\boldsymbol{\sigma}_r^2 = \left[\sigma_{r1}^2, \cdots, \sigma_{rL}^2\right]^T$ is the variance vector of the rth endmember, $\boldsymbol{M} = [\boldsymbol{m}_1, \cdots, \boldsymbol{m}_R]$ is the $(L \times R)$ matrix containing the endmember means of the image, $\boldsymbol{e}_n \sim \mathcal{N}\left(\boldsymbol{0}_L, \psi_n^2\mathbf{I}_L\right)$ is an additive residual Gaussian noise, $\psi_n \in \mathbb{R}$, $\boldsymbol{0}_L$ is an $(L \times 1)$ vector of 0 and $\mathbf{I}_L$ is the $(L \times L)$ identity matrix. The abundance vector $\boldsymbol{a}_n$ contains proportions and thus should satisfy the physical positivity and sum-to-one (PSTO) constraints $a_{rn} \geq 0, \forall r \in \{1, \ldots, R\}$ and $\sum_{r=1}^{R} a_{rn} = 1$.

There are several motivations for considering the GNCM. First, model (1) accounts for EV by considering a Gaussian distribution, whose variances $\boldsymbol{\sigma}_r^2$ change from one spectral band to another, for each physical component in the image. This allows the GNCM to capture the spectral variations of each physical element with respect to each spectral band. Second, model (1) generalizes the LMM

This work was supported in part by the HYPANEMA ANR Project under Grant ANR-12-BS03-003, and in part by the Thematic Trimester on Image Processing of the CIMI Labex, Toulouse, France, under Grant ANR-11-LABX-0040-CIMI within the Program ANR-11-IDEX-0002-02.

model since the GNCM reduces to the LMM for $\boldsymbol{\sigma}_r^2 = \mathbf{0}_L, \ \forall r$. Third, model (1) generalizes the NCM since it introduces an additional residual Gaussian noise $\boldsymbol{e}$ that makes the proposed model more robust with respect to mismodeling. Note that the GNCM reduces to the NCM for $\psi_n^2 = 0, \ \forall n$. To summarize, the main motivations for studying model (1) is that it generalizes the standard LMM and NCM and allows EV to be taken into account.

2.2. Likelihood

Using the observation model (1), the Gaussian properties of both the noise sequence $\boldsymbol{e}_n$ and the endmembers, and exploiting independence between the noise samples in different spectral bands, yield the following likelihood

$$f(\boldsymbol{y}_n|\boldsymbol{A},\boldsymbol{M},\boldsymbol{\Sigma},\boldsymbol{\Psi}) \propto \left(\prod_{\ell=1}^{L}\boldsymbol{\Lambda}_{\ell n}\right)^{\frac{1}{2}} \times \exp\left\{-\frac{1}{2}\boldsymbol{\Lambda}_{:n}^{T}\left[(\boldsymbol{y}_n-\boldsymbol{M}\boldsymbol{a}_n)\odot(\boldsymbol{y}_n-\boldsymbol{M}\boldsymbol{a}_n)\right]\right\} \quad (2)$$

where $\boldsymbol{\Lambda}$ is an $(L \times N)$ matrix whose elements are given by $\boldsymbol{\Lambda}_{\ell n} = \left(\sum_{r=1}^{R} a_{rn}^2\sigma_{r\ell}^2 + \psi_n^2\right)^{-1}$, $\boldsymbol{A} = [\boldsymbol{a}_1,\cdots,\boldsymbol{a}_N]$ is an $(R \times N)$ abundance matrix, N is the number of pixels, $\boldsymbol{\Sigma} = \left(\sigma_{r,l}^2\right)_{r=1,\ldots,R,l=1,\ldots,L}$ is an $(R \times L)$ matrix, $\boldsymbol{\Psi} = [\psi_1,\ldots,\psi_N]$ is an $(1 \times N)$ vector and $\odot$ denotes the Hadamard (termwise) product. Note that the elements of $\boldsymbol{\Lambda}$ depend jointly on the noise variances, the endmember variances and the pixel abundances contrary to the LMM.

2.3. Parameter/hyperparameter priors

The likelihood defined in (2) depends on the unknown parameters $\boldsymbol{M}$ (endmember matrix), $\boldsymbol{A}$ (abundance matrix), $\boldsymbol{\Sigma}$ (endmember variances) and $\boldsymbol{\Psi}$ (noise variances). In order to promote spatial correlations between adjacent pixels of the image, we proposed in [8,9] to introduce $(1 \times N)$ label vectors $\boldsymbol{z}$ indicating the classes of the image pixels. The abundances were then assigned priors depending on these labels and on the $(R \times K)$ matrix of Dirichlet parameters $\boldsymbol{C} = [\boldsymbol{c}_1,\cdots,\boldsymbol{c}_K]$ associated with these K classes. All these prior distributions are briefly recalled below (see also [8,9]):

• **Label prior**: $f(\boldsymbol{z}) = \frac{1}{G(\beta)}\exp\left[\beta\sum_{n=1}^{N}\sum_{n'\in\nu(n)}\delta(z_n - z_{n'})\right]$ where $\beta > 0$ is the granularity coefficient, $\nu(n)$ denotes the pixel neighborhood, $G(\beta)$ is a normalizing (or partition) constant and $\delta(.)$ is the Dirac delta function (see [11] for a similar choice),

• **Abundance prior**: $f(\boldsymbol{A}|\boldsymbol{z},\boldsymbol{C}) = \prod_{n=1}^{N} f(\boldsymbol{a}_n|z_n = k,\boldsymbol{c}_k)$ where $\boldsymbol{a}_n|z_n = k,\boldsymbol{c}_k \sim \text{Dir}(\boldsymbol{c}_k)$, for $n \in \mathcal{I}_k$, Dir(.) denotes the Dirichlet distribution, and $n \in \mathcal{I}_k$ means that $\boldsymbol{y}_n$ belongs to the kth class (which is also equivalent to $z_n = k$),

• **Endmember mean prior**: $f(\boldsymbol{M}) = \prod_{n=1}^{R} f(\boldsymbol{m}_r)$, with $\boldsymbol{m}_r \sim \mathcal{N}_{[0,1]^L}\left(\widetilde{\boldsymbol{m}}_r, \epsilon^2\mathbf{I}_L\right)$, where $\mathcal{N}_I$ denotes a truncated Gaussian distribution on I, $\widetilde{\boldsymbol{m}}_r$ is an estimated endmember (resulting from an endmember extraction algorithm such as VCA [14]) and ϵ^2 is a fixed variance term defining the confidence that we have on this estimated endmember $\widetilde{\boldsymbol{m}}_r$,

• **Endmember variance prior**: $f(\boldsymbol{\Sigma}) \propto \prod_{\ell=1}^{L}\prod_{r=1}^{R}\frac{1}{\sigma_{rl}^2}\mathbf{1}_{\mathbb{R}+}\left(\sigma_{rl}^2\right)$

• **Noise variance prior**: $f(\boldsymbol{\Psi}|\lambda) = \prod_{n=1}^{N}\lambda\exp\left(-\lambda\psi_n^2\right)\mathbf{1}_{\mathbb{R}+}\left(\psi_n^2\right)$ where λ has a large value ensuring sparsity for ψ_n ($\lambda = 10^7$ in our simulations).

• **Dirichlet parameters**: $\boldsymbol{c}_k$ was assigned a conjugate prior as defined in [15] in order to ensure a non-informative prior (flat distribution) (see [8] for more details).

2.4. Posterior distribution

The parameters of the proposed Bayesian model are included in the vector $\boldsymbol{\theta} = \{\boldsymbol{\theta}_p,\boldsymbol{\theta}_h\}$ where $\boldsymbol{\theta}_p = \{\boldsymbol{A},\boldsymbol{M},\boldsymbol{\Sigma},\boldsymbol{\Psi}\}$ (parameters) and $\boldsymbol{\theta}_h = \{\boldsymbol{C},\boldsymbol{z}\}$ (hyperparameters). The joint posterior distribution of the unknown parameter/hyperparameter vector $\boldsymbol{\theta}$ can be computed from the following hierarchical structure

$$f(\boldsymbol{\theta}_p,\boldsymbol{\theta}_h|\boldsymbol{Y}) \propto f(\boldsymbol{Y}|\boldsymbol{\theta}_p)\,f(\boldsymbol{\theta}_p|\boldsymbol{\theta}_h)\,f(\boldsymbol{\theta}_h) \quad (3)$$

where $f(\boldsymbol{\theta}_p,\boldsymbol{\theta}_h) = f(\boldsymbol{\theta}_p|\boldsymbol{\theta}_h)\,f(\boldsymbol{\theta}_h) = f(\boldsymbol{A}|\boldsymbol{C},\boldsymbol{z})\,f(\boldsymbol{M})\,f(\boldsymbol{\Sigma})\,f(\boldsymbol{\Psi})\,f(\boldsymbol{C}|\boldsymbol{z})\,f(\boldsymbol{z})$, resulting from prior independence between the different parameters.

Unfortunately, it is difficult to obtain closed form expressions for the standard Bayesian estimators associated with (3). These estimators are therefore approximated using an MCMC approach that generates samples asymptotically distributed according to (3). This is achieved using a hybrid Gibbs sampler that sequentially samples the following parameters of interest $\boldsymbol{A}$, $\boldsymbol{M}$, $\boldsymbol{\Sigma}$, $\boldsymbol{z}$, $\boldsymbol{\Psi}$ and $\boldsymbol{C}$, according to their conditional distributions [16]. Due to the large number of parameters to be sampled and to the complexity of the conditional distributions, we use a CHMC algorithm with good mixing properties [12]. The parameters are finally estimated using the MMSE estimator for $\{\boldsymbol{A},\boldsymbol{M},\boldsymbol{\Sigma},\boldsymbol{\Psi},\boldsymbol{C}\}$ and the MAP estimator for the labels $\boldsymbol{z}$. The reader is invited to consult [8] for more details.

3. SIMULATION RESULTS ON REAL DATA

The main contribution of this paper is a performance evaluation of the mixing model (1) and its estimation algorithm (referred to as UsGNCM) when applied to a real HS data set, which is the objective of this section. The considered real image was acquired in 2010 by the Hyspex HS scanner over Villelongue, France. The dataset contains $L = 160$ spectral bands, 100×100 pixels and $R = 4$ components: tree, grass, soil and shadow (see Fig. 1 (a)). Our algorithm is compared with: (i) VCA+FCLS: [14,17], (ii) UsLMM [18] and (iii) AEB [19] (used with 10% image subset and the VCA algorithm).

3.1. Endmember and variability estimation

The UsGNCM algorithm estimates both the mean and variance of each physical element in the scene which provides an EV measure in the considered image. Fig. 2 shows the estimated endmember distributions as blue level areas for each endmember. These distributions are in good agreement with the estimates obtained with VCA, AEB and UsLMM algorithms except for the shadow endmember. Indeed, both AEB and VCA provide a different shadow endmember because they extract the endmembers from the image pixels while UsLMM and UsGNCM estimate both the abundances and endmembers resulting in a better shadow estimate (of lower amplitude). Note finally that the variation is more pronounced for high spectral bands ($l > 80$) which is in agreement with the results presented in [13].

3.2. Abundance Estimation and Image Classification

The fraction maps estimated by the different methods are shown in Fig. 3. Note that a white (black) pixel indicates a large (small) proportion of the corresponding materials. These maps lead to the following conclusions

- UsLMM and UsGNCM present similar abundance estimates with a smoother behavior for the second algorithm (because considering spatial correlations)

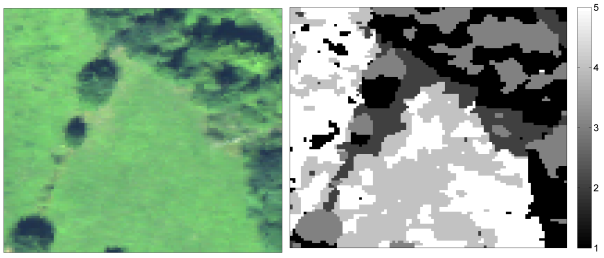

(a) Madonna image. (b) Classification map.

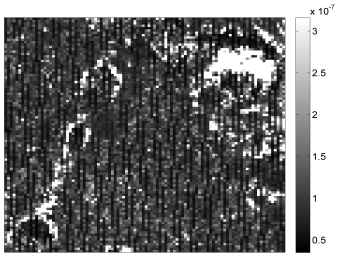

(c) Noise variances.

Fig. 1. (a) Real Madonna image, (b) the estimated classification map using UsGNCM and (c) noise variances.

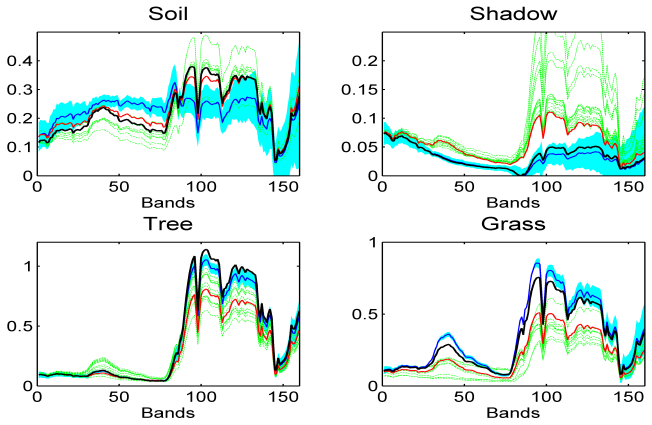

Fig. 2. The $R = 4$ endmembers estimated by VCA (red lines), UsLMM (black lines), AEB (green lines), UsGNCM (blue lines) and the estimated endmember distribution (blue level areas) for the Madonna image.

- The abundance maps of VCA-FLCS, AEB are higher than those of statistical methods (UsLMM and UsGNCM) especially for the "shadow" and "tree" classes. Indeed, VCA-FCLS and AEB assume the presence of pure pixels in the image which is not true for the shadow (the shadow pixels in the image are tree-shadowed pixels which should not be considered as pure pixels)
- AEB is sensitive to the similarity between tree and grass spectra leading to inaccurate grass maps.

In addition to unmixing, UsGNCM also provides a spatial segmentation of the considered scene as shown in Fig. 1(b). This classification map clearly highlights the area of each physical element in the scene. Indeed, we have 5 classes that represent tree, soil, shadow and two kinds of grass. Table 1 finally reports the estimated Dirichlet parameters and the number of pixels for each spatial class when considering the Madonna image. These parameters suggest a highly non uniform distribution over the simplex which can explain the good performance of the proposed approach.

Table 1. Estimated Dirichlet parameters for the Madonna image.

	Dirichlet parameters				number of pixels
	$\hat{c}_{1k}$	$\hat{c}_{2k}$	$\hat{c}_{3k}$	$\hat{c}_{4k}$	
$k=1$	1.47	4.59	10.98	4.39	2144
$k=2$	13.26	14.05	15.96	14.22	1064
$k=3$	0.76	7.97	3.75	1.36	1502
$k=4$	37.71	76.11	84.06	99.97	2483
$k=5$	23.04	57.70	89.82	99.93	2807

3.3. Noise variances

The proposed algorithm also provides a measure of the noise variance for each observed pixel. This parameter brings an information about pixels that are inaccurately described by the linear mixing model, i.e., allows modeling errors to be quantified. Fig. 1 (c) shows the obtained noise variances for the considered image. This figure shows a higher error in the shadow area and around trees, i.e., for regions where possible interactions between physical components might occur (e.g., tree/soil) resulting in a more complex model than the proposed linear one. Note finally that Fig. 1 (c) highlights the presence of regular vertical patterns that have also been observed in [20] and were associated with a sensor defect or other miscalibration problems.

4. CONCLUSIONS

This paper introduced a Bayesian model for unsupervised unmixing of HS images accounting for EV. The proposed model was based on a generalization of the NCM defined by the endmembers of the scene, their variability controlled by a scale parameter (variance) and the abundances for each pixel of the scene. The observed image was also spatially classified into regions sharing homogeneous abundance characteristics. The physical constraints about the abundances were ensured by choosing a Dirichlet distribution for each spatial class of the image. Due to the complexity of the resulting joint posterior distribution, an MCMC procedure (based on a hybrid Gibbs sampler) was used to sample the posterior of interest and to approximate the Bayesian estimators of the unknown parameters using the generated samples. The proposed algorithm showed good performance when processing real data presenting EV and spatial correlation between adjacent image pixels. It was also shown to be robust to the absence of pure pixels in the observed scene. Future work includes the introduction of endmember variability in nonlinear mixing models.

5. REFERENCES

[1] N. Dobigeon, J.-Y. Tourneret, C. Richard, J.C.M. Bermudez, S. McLaughlin, and A.O. Hero, "Nonlinear unmixing of hyperspectral images: Models and algorithms," *IEEE Signal Process. Mag.*, vol. 31, no. 1, pp. 82–94, Jan 2014.

[2] B. Somers, G. P. Asner, L. Tits, and P. Coppin, "Endmember variability in spectral mixture analysis: A review," *Remote Sens. Environ.*, vol. 115, no. 7, pp. 1603 – 1616, 2011.

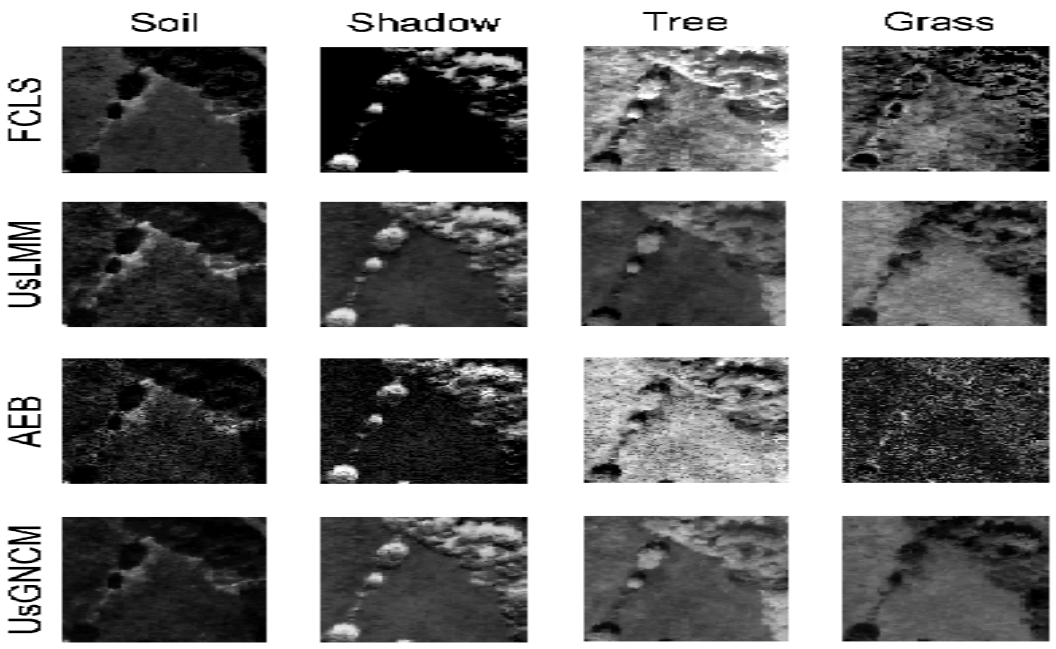

Fig. 3. Abundance maps estimated by FCLS (first row), UsLMM (second row), AEB (third row) and the proposed UsGNCM (fourth row) for the Madonna image.

[3] A. Zare and K.C. Ho, "Endmember variability in hyperspectral analysis: Addressing spectral variability during spectral unmixing," *IEEE Signal Process. Mag.*, vol. 31, no. 1, pp. 95–104, Jan 2014.

[4] X. Du, A. Zare, P. Gader, and D. Dranishnikov, "Spatial and spectral unmixing using the beta compositional model," *IEEE J. Sel. Topics Appl. Earth Observat. Remote Sens.*, vol. 7, no. 6, pp. 1994–2003, June 2014.

[5] D. Stein, "Application of the normal compositional model to the analysis of hyperspectral imagery," in *Proc. IEEE Workshop Adv. Techniques for Analysis of Remotely Sensed Data*, Oct 2003, pp. 44–51.

[6] O. Eches, N. Dobigeon, C. Mailhes, and J.-Y. Tourneret, "Bayesian estimation of linear mixtures using the normal compositional model. Application to hyperspectral imagery," *IEEE Trans. Image Process.*, vol. 19, no. 6, pp. 1403–1413, June 2010.

[7] A. Zare, P. Gader, and G. Casella, "Sampling piecewise convex unmixing and endmember extraction," *IEEE Trans. Geosci. Remote Sens.*, vol. 51, no. 3, pp. 1655–1665, March 2013.

[8] A. Halimi, N. Dobigeon, and J.-Y. Tourneret, "Unsupervised unmixing of hyperspectral images accounting for endmember variability," in *ArXiv e-prints*, Jun. 2014.

[9] A. Halimi, N. Dobigeon, J.-Y. Tourneret, and P. Honeine, "A new Bayesian unmixing algorithm for hyperspectral images mitigating endmember variability," in *Proc. IEEE Int. Conf. Acoust., Speech, and Signal Process. (ICASSP)*, Brisbane, Australia, April 2015, to appear.

[10] N. Bali and A. Mohammad-Djafari, "Bayesian approach with hidden markov modeling and mean field approximation for hyperspectral data analysis," *IEEE Trans. Image Process.*, vol. 17, no. 2, pp. 217–225, Feb. 2008.

[11] O. Eches, N. Dobigeon, and J.-Y. Tourneret, "Enhancing hyperspectral image unmixing with spatial correlations," *IEEE Trans. Geosci. Remote Sens.*, vol. 49, no. 11, Nov 2011.

[12] S. Brooks, A. Gelman, G. L . Jones, and X.-L. Meng, *Handbook of Markov chain Monte Carlo*, ser. Chapman & Hall/CRC Handbooks of Modern Statistical Methods. Taylor & Francis, 2011.

[13] Y. Altmann, N. Dobigeon, S. McLaughlin, and J.-Y. Tourneret, "Unsupervised post-nonlinear unmixing of hyperspectral images using a Hamiltonian Monte Carlo algorithm," *IEEE Trans. Image Process.*, vol. 23, no. 6, pp. 2663–2675, June 2014.

[14] J. M. P. Nascimento and J. M. Bioucas-Dias, "Vertex component analysis: A fast algorithm to unmix hyperspectral data," *IEEE Trans. Geosci. Remote Sens.*, vol. 43, no. 4, pp. 898–910, April 2005.

[15] Z. Ma, "Bayesian estimation of the Dirichlet distribution with expectation propagation," in *Proc. European Signal Process. Conf. (EUSIPCO)*, Bucharest, Romania, Aug. 2012.

[16] C. P. Robert, *The Bayesian Choice: from Decision-Theoretic Motivations to Computational Implementation*, Springer Texts in Statistics. Springer-Verlag, New York, 2 edition, 2007.

[17] D. C. Heinz and C. -I Chang, "Fully constrained least-squares linear spectral mixture analysis method for material quantification in hyperspectral imagery," *IEEE Trans. Geosci. Remote Sens.*, vol. 29, no. 3, pp. 529–545, March 2001.

[18] N. Dobigeon, S. Moussaoui, M. Coulon, J.-Y. Tourneret, and A. O. Hero, "Joint Bayesian endmember extraction and linear unmixing for hyperspectral imagery," *IEEE Trans. Signal Process.*, vol. 57, no. 11, pp. 4355–4368, Nov. 2009.

[19] B. Somers, M. Zortea, A. Plaza, and G.P. Asner, "Automated extraction of image-based endmember bundles for improved spectral unmixing," *IEEE. J. Sel. Topics Appl. Earth Observat. Remote Sens.*, vol. 5, no. 2, pp. 396–408, April 2012.

[20] C. Févotte and N. Dobigeon, "Nonlinear hyperspectral unmixing with robust nonnegative matrix factorization," in *ArXiv e-prints*, March 2014.